High-resolution spectroscopy and quantum-defect model for the gerade triplet np and nf Rydberg states of He2

Author(s):
Sprecher, Daniel; Liu, Jinjun; Krähenmann, Tobias; Schäfer, Martin; Merkt, Frédéric

Publication date:
2014

Permanent link:
https://doi.org/10.3929/ethz-b-000081379

Originally published in:
The Journal of Chemical Physics 140(6), https://doi.org/10.1063/1.4864002

Funding acknowledgement:
146759 - Rydberg states, VUV laser spectroscopy and photoionization dynamics (SNF)

The following article appeared in *J. Chem. Phys.* **140**, 064304 (2014) and may be found at http://dx.doi.org/10.1063/1.4864002.

An accurate quantum-defect model for the triplet np Rydberg states of He_2

Daniel Sprecher,[1] Jinjun Liu,[1, a)] Tobias Krähenmann,[1] Martin Schäfer,[1] and Frédéric Merkt[1, b)]

Laboratorium für Physikalische Chemie, ETH-Zürich, 8093 Zürich, Switzerland

(Dated: 19 November 2019)

Photoionization spectra and Rydberg-state-resolved threshold-ionization spectra of triplet np Rydberg states of $^4He_2$ located in the vicinity of the $X^+\,^2\Sigma_u^+\,(v^+ = 0)$ ionization threshold were recorded from the $2s\sigma\,a\,^3\Sigma_u^+$ metastable state. An accuracy of $0.01\,cm^{-1}$ was achieved for the experimental term values of the observed Rydberg states. The data were combined with spectroscopic data on low-lying triplet np and nf Rydberg states from the literature to derive energy- and internuclear-distance-dependent eigenquantum-defect parameters of multichannel quantum-defect theory (MQDT). The MQDT calculations reproduce the experimental data within their experimental uncertainties and enabled the derivation of potential-energy curves for the lowest triplet p Rydberg states ($n = 2 - 5$) of He_2. The eigenquantum-defect parameters describing the p-f interaction were found to be larger than 0.002 at the energies corresponding to the high-n Rydberg states, so that the p-f interaction plays an important role in the autoionization dynamics of np Rydberg states with $v^+ = 0$. By extrapolating the experimental term values of triplet np Rydberg states of $^4He_2$ in the range of principal quantum number n between 87 and 110, the positions of the $(v^+ = 0, N^+ = 3)$ and $(v^+ = 0, N^+ = 5)$ levels of the ground state of $^4He_2^+$ were determined to lie $70.937(3)\,cm^{-1}$ and $198.369(6)\,cm^{-1}$, respectively, above the $(v^+ = 0, N^+ = 1)$ ground rotational level.

PACS numbers: 33.80.Rv, 33.80.Eh, 33.60.+q, 33.20.Wr, 33.20.Tp, 33.20.Sn, 33.15.Ry
Keywords: helium dimer, Rydberg-state-resolved threshold-ionization spectroscopy, rotational and vibrational channel interactions, p-f interaction, field-induced autoionization, He_2^+

[a)] Present address: Department of Chemistry and Conn Center for Renewable Energy Research, University of Louisville, Louisville, Kentucky 40292, USA

[b)] Electronic mail: frederic.merkt@phys.chem.ethz.ch

I. INTRODUCTION

Atomic helium has the lowest polarizability[1] ($0.205\,\text{Å}^3$) and the largest ionization energy[2] ($198\,310.6664(2)\,\text{cm}^{-1}$) of all neutral elements and is chemically very inert.[3] The potential-energy well of He_2 in the $X\,^1\Sigma_g^+$ ground state is so shallow that it only supports a single quantum state ($v = 0, N = 0$) for $^4He_2$ with a dissociation energy $D_0(^4He_2) = 0.00112(2)\,\text{cm}^{-1}$.[4–6] The $X^+\,^2\Sigma_u^+$ ground state of He_2^+ corresponds to the electronic configuration $(1s\sigma_g)^2(1s\sigma_u)^1$. He_2^+ therefore has a covalent bond of order ½ with a Born-Oppenheimer binding energy $D_e(He_2^+) = 19\,954.583\,\text{cm}^{-1}$.[7]

The rovibrational energy levels of He_2^+ serve as benchmark quantities for *ab initio* calculations of three-electron systems.[7–16] In contrast to the numerous theoretical studies reported on He_2^+, only a few experimental studies have been carried out. For the main naturally occurring isotopomer, $^4He_2^+$, no electric-dipole-allowed rotational and vibrational spectra exist. Yu and Wing[17] observed nine transitions in the fundamental vibrational band of the heteronuclear $^3He^4He^+$ isotopomer, which exhibits a small electric dipole moment. Carrington *et al.*[11] measured the frequency of seven electronic transitions from vibrationally highly excited levels of the $X^+\,^2\Sigma_u^+$ ground state of $^4He_2^+$ to the weakly bound $A^+\,^2\Sigma_g^+$ first excited state. Raunhardt *et al.*[18] determined rotational constants for the lowest three vibrational levels of $^4He_2^+$ and observed the rotational structure of the ground state of $^3He_2^+$ by pulsed-field-ionization zero-kinetic-energy (ZEKE) photoelectron spectroscopy of metastable He_2. Experimental results obtained by Hardy and coworkers[19] on the rotational structure of $^4He_2^+$ have been questionned because their analysis is based on the observation of states which do not fulfill the generalized Pauli principle (see also discussion in Refs. 18, 20, and 21).

Ginter and coworkers[22–26], and also Raunhardt *et al.*[18], measured the term values of triplet np Rydberg states of He_2 and obtained rovibrational energy spacings in He_2^+ by extrapolation to the series limits using MQDT. Their model included rotational channel interactions and the dependence of the eigenquantum-defect parameters on the energy, the rotational quantum number, and the vibrational quantum number. The accuracy of the extrapolated energies presented in Refs. 23 and 18 was limited to about $0.1\,\text{cm}^{-1}$. In the experiments presented in this article, an accuracy of $0.01\,\text{cm}^{-1}$ was achieved in the determination of the term values of high-np Rydberg states of $^4He_2$ and in the extrapolation of the observed Rydberg series to their limits using an extended MQDT model. This model includes internuclear-

distance- and energy-dependent eigenquantum-defect functions and considers the effects of the p-f interaction, which is known to induce perturbations in the structure of the np and nf Rydberg states of He_2.[23,27] Using this model, a global description of the triplet np Rydberg states of He_2 was achieved in a fit of the relevant MQDT parameters to spectroscopic data available in the literature.[22–29] With this improved model, the positions of all known triplet np Rydberg states can be calculated within their experimental uncertainties, Born-Oppenheimer potential-energy curves of the 2–5 p Rydberg states were derived, and the corresponding leading adiabatic corrections were estimated.

II. EXPERIMENT

A. Production and photoionization spectroscopy of He_2

A schematic diagram of the experimental chamber is shown in Fig. 1. It consists of a gas source chamber and a photoexcitation/detection chamber separated by a skimmer with an orifice diameter of 1 mm. A supersonic beam containing $^4He_2$ in the $2s\sigma\, a\,^3\Sigma_u^+$ metastable state (referred to as He_2^* hereafter) was produced from atomic helium by striking an electric discharge at the orifice of a pulsed nozzle. The discharge design has been described in detail previously.[18] The phosphorescence-limited lifetime of He_2^* is 13(2) s,[30] which is much longer than the time ($\sim 150\,\mu$s) required for the metastable molecules to reach the photoexcitation region. The photoexcitation region was surrounded by a cylindrically symmetric stack of resistively coupled metallic electrodes designed for the application of homogeneous electric fields and by two concentric magnetic shields made of mu-metal to suppress stray magnetic fields. Differential pumping resulted in background pressures of 10^{-4} mbar and 5×10^{-7} mbar in the gas source chamber and the photoexcitation/detection chamber, respectively.

Triplet np Rydberg states of He_2 were excited from He_2^* using the third harmonic (wavelength 292 nm, pulse length 30 ns, bandwidth $< 0.001\,\mathrm{cm}^{-1}$, pulse energy $\sim 150\,\mu$J) of the output of a Ti:Sa laser system described in Ref. 31. A pulsed homogeneous electric field (amplitude 128 V/cm) was generated 200 ns after laser excitation by applying a pulsed voltage across the electrode stack. The electric field was used to ionize Rydberg states and its polarity was chosen such that the positively charged ions were accelerated towards a microchannel-plate (MCP) detector. The ion signal corresponding to the time of flight of

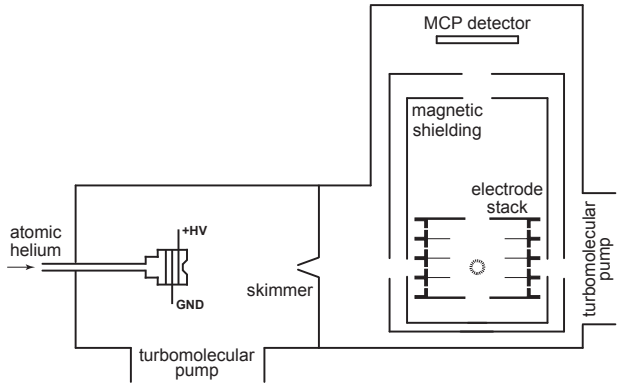

FIG. 1. Schematic diagram of the vacuum chambers used in the experiments. The photoexcitation region is marked with a circle.

the He_2^+ ions was integrated and monitored as a function of the laser wave number.

B. Rydberg-state-resolved threshold-ionization spectroscopy

He_2^* molecules in many different rovibrational states are produced in the electric discharge and the Rydberg series excited from these states and observed in the photoionization (PI) spectra overlap, which makes unambiguous assignments very difficult. By changing to the detection scheme of Rydberg-state-resolved threshold-ionization (RSR-TI) spectroscopy,[32] which restricts the detection to electrons produced by field ionization of long-lived Rydberg states, the spectral congestion could be considerably reduced. In RSR-TI spectroscopy, a longer delay ($2\,\mu$s in the present case) and an electric field of smaller amplitude ($12.8\,$V/cm) and opposite polarity compared to PI spectroscopy are used to field-ionize the Rydberg states. The spectra are recorded by monitoring the electron signal detected on the MCP detector as a function of the laser wave number. Electrons originating from direct photoionization or from autoionizing Rydberg states with lifetimes shorter than $2\,\mu$s leave the photoexcitation region before the electric-field pulse is applied and are not detected. RSR-TI spectroscopy was already applied in our group to study high-n Rydberg states of N_2,[32] NH_3,[33] and Kr[34] and the corresponding cationic states at high resolution.

TABLE I. List of contributions to the absolute and relative uncertainties in the determination of the transition wave numbers. All values are given in units of cm^{-1}.

Source of uncertainty	Uncertainty in UV
Calibration of absolute wave numbers	
Positions of iodine reference lines[35]	0.009
Doppler shift	0.004
Frequency shift in the Ti:Sa amplifier	< 0.001
Pressure shift	< 0.001
Total absolute uncertainty[a]	0.010
Calibration of relative wave numbers	
Calibration of relative laser frequency	0.006[b]
Determination of the line centers	0.001
Stark shifts	< 0.001[c]
Total relative uncertainty[a]	0.006[b]

[a] Determined by summation of all contributions in quadrature.

[b] Assuming that the transitions are separated by $\sim 12\,\mathrm{cm}^{-1}$. Because the relative laser frequency is determined by extrapolation, the uncertainty is proportional to the interval (see text).

[c] This value was estimated for np Rydberg states with $n < 50$. At higher values of n, the dc Stark shifts can be larger.

C. Wave-number calibration

For the absolute wave-number calibration, iodine absorption spectra were recorded simultaneously with the PI and RSR-TI spectra of He_2^* using part of the fundamental cw radiation near 876 nm. The transition wave numbers of selected lines tabulated in the iodine atlas of Gerstenkorn and coworkers[35] served as reference, resulting in an estimated uncertainty in the absolute wave-number calibration of $0.003\,\mathrm{cm}^{-1}$ in the fundamental near-infrared radiation and $0.009\,\mathrm{cm}^{-1}$ in the upconverted ultraviolet (UV) radiation. Although the iodine cell was heated up to 800 °C, the signal was too weak to record saturated Doppler-free I_2 spectra, which would have allowed for a more accurate wave-number calibration.

Relative laser wave numbers were determined using the transmission signal through a frequency-stabilized high-finesse Fabry-Pérot etalon. The free spectral range (FSR) of this etalon was determined in Ref. 36 to be 149.969(1) MHz using radiation at 792 nm. This value was found to also be valid within 0.03 MHz at 876 nm using iodine absorption spectroscopy as described above. A FSR of 149.969(30) MHz was therefore used in the present study. Because the relative wave-number calibration is limited by the uncertainty of the FSR of the etalon, the uncertainty in the relative positions of two transitions is proportional to

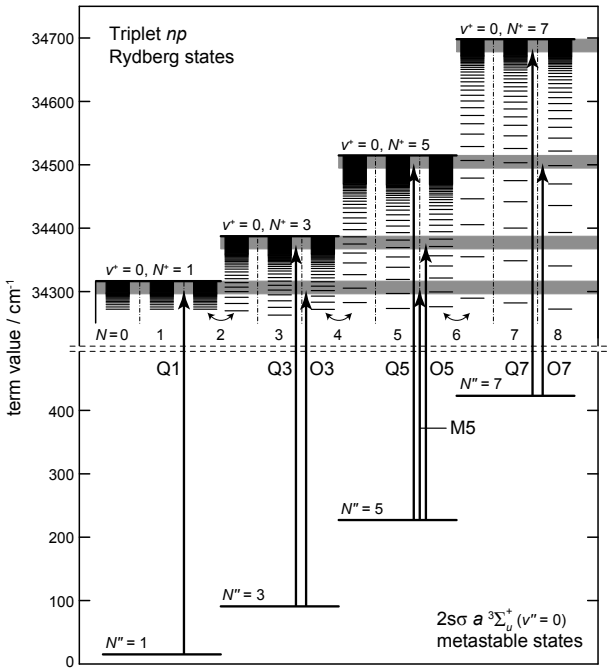

FIG. 2. Energy-level diagram of the rotational levels of $^4He_2^*$ and the triplet np Rydberg states of $^4He_2$. The regions shaded in gray are those probed by RSR-TI spectroscopy using electric-field pulses of 12.8 V/cm. The vertical arrows designate the eight spectral regions investigated in the present study. The origin of the wave-number scale was placed at the position of the origin of the $2s\sigma\, a\, ^3\Sigma_u^+$ state which corresponds to the position of the Pauli-forbidden ($v'' = 0, N'' = 0, J'' = 1$) level.

their separation. For typical separations of less than $12\,\mathrm{cm}^{-1}$, the relative uncertainty in the determination of transition wave numbers is estimated to be less than $0.006\,\mathrm{cm}^{-1}$. All contributions to the estimated total absolute and relative uncertainties of $0.01\,\mathrm{cm}^{-1}$ and $0.006\,\mathrm{cm}^{-1}$, respectively, are listed in Table I. The systematic uncertainties resulting from Doppler shifts, pressure shifts, and Stark shifts were estimated as described in Ref. 37.

III. RESULTS

A. Observed transitions and their assignment

A schematic energy level diagram of the initial metastable states and final triplet np Rydberg states investigated in the present study is depicted in Fig. 2. When neglecting channel interactions, the spectral positions $\tilde{\nu}$ of Rydberg states are well described by the

Rydberg formula

$$\tilde{\nu} = \frac{E^+(v^+, N^+)}{hc} - \frac{\mathcal{R}_{\mathrm{He_2}}}{(n - \bar{\mu})^2}, \tag{1}$$

where h is Planck's constant, c is the speed of light in vacuum, $E^+(v^+, N^+)$ are the energies of the rovibrational ionization thresholds, $\mathcal{R}_{\mathrm{He_2}} = 109\,729.796\,\mathrm{cm}^{-1}$ is the mass-corrected Rydberg constant, and $\bar{\mu}$ is the effective quantum defect. Rydberg states with even values of N^+ do not exist because their wave function would be antisymmetric with respect to the permutation of the two bosonic $^4\mathrm{He}^{2+}$ nuclei and therefore violate the generalized Pauli principle. For the same reason, rotational levels of the metastable state with even values of N'' do not exist.

The pulsed electric field used to ionize the Rydberg states when recording the RSR-TI spectra had an amplitude of 12.8 V/cm, which lowers the ionization thresholds by $\sim 20\,\mathrm{cm}^{-1}$ and restricts the energetic detection windows to the regions marked by areas shaded in gray in Fig. 2. Eight spectral regions, marked by vertical arrows in Fig. 2, were investigated at high spectral resolution. These regions are identified using the labels Q1, Q3, Q5, Q7, O3, O5, O7, and M5 which designate the different ionization thresholds according to the change in the rotational quantum number $\Delta N = N^+ - N''$ and the value of N''. Regions which correspond to $\Delta N = 0, -2$, and -4 transitions are labeled using the letters 'Q', 'O', and 'M', respectively. The present investigation was restricted to transitions with $v'' = v^+ = 0$. For a given value of N^+, three np Rydberg series can be observed with $N = N^+ - 1, N^+$, and $N^+ + 1$. Throughout this article, the notation $N'' \rightarrow n\,\ell\,N_N^+$ is used to label transitions from the rotational levels of the $2s\sigma\,a\,^3\Sigma_u^+\,(v'' = 0, N'')$ metastable states to triplet $n\,\ell\,N_N^+\,(v^+ = 0)$ Rydberg states.

As illustrations of the data obtained experimentally, representative sections of the PI and RSR-TI spectra recorded in regions Q5 and O7 are depicted in panels (a) and (b) of Fig. 3, respectively. The corresponding etalon transmission spectra and iodine absorption spectra used for calibration are also displayed. The intensities of the etalon transmission lines fluctuate because the step size of the laser was comparable to their linewidth. In the PI spectrum (top trace in Fig. 3a), the expected transitions from the $(v'' = 0, N'' = 5)$ level of the metastable state to high-np Rydberg states with $N^+ = 5$ (see assignment bars) are obscured by transitions from higher-lying rovibrational levels of the metastable state to autoionizing low-np Rydberg states. In the corresponding RSR-TI spectrum, only the $np5_6$

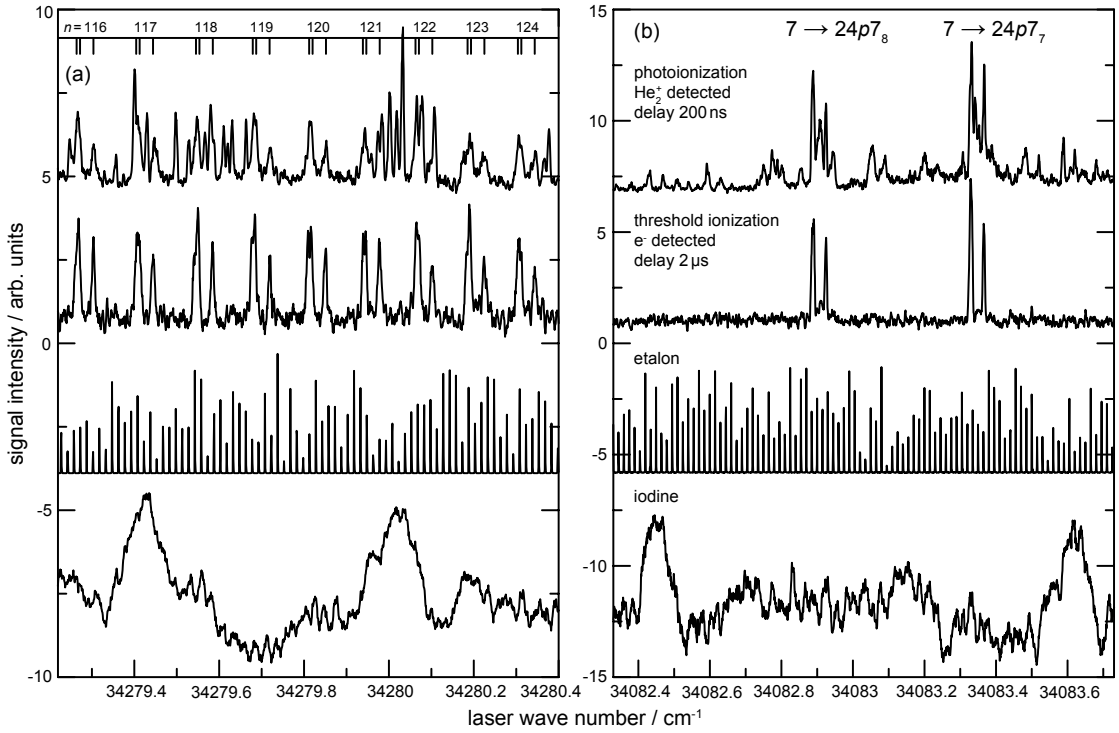

FIG. 3. Comparison between the PI spectra (top trace) and the RSR-TI spectra (second trace from top) recorded in (a) region Q5 and (b) region O7 (see Fig. 2 for the definition of these regions). Simultaneously with the He_2 spectra, etalon traces (third trace from top) and iodine spectra (bottom trace) were recorded for the relative and absolute frequency calibrations, respectively (shifted along the vertical axis for clarity). In panel (a) the transitions are labeled with the principal quantum number n of the $5 \rightarrow np5_6$ series.

Rydberg series is visible because the delayed detection of electrons (delay $2\,\mu$s) prevents Rydberg states with lifetimes $\ll 2\,\mu$s from being detected. The splitting observed for each $5 \rightarrow np5_6$ transition originates from the fine structure of the initial metastable state, as discussed in Section III B. The $np5_4$ and $np5_5$ Rydberg series are not observed in region Q5 of the RSR-TI spectrum, for reasons that are discussed in Section III F.

The PI and RSR-TI spectra in region O7 displayed in Fig. 3b are dominated by the $N = 7$ and $N = 8$ orbital fine-structure components of the $7 \rightarrow np7_N$ series which were assigned on the basis of the calculations presented in Ref. 18. The $24p7_N$ Rydberg states are located about $192\,\mathrm{cm}^{-1}$ below the $N^+ = 7$ ionization threshold (see Fig. 2) and it may seem surprising, at first sight, that these states are at all field ionized by the 12.8 V/cm pulsed electric field used to record the RSR-TI spectrum. The observation can be explained by the mechanism of field-induced rotational autoionization:[38,39] The $24p7_N$ Rydberg states are located about $9\,\mathrm{cm}^{-1}$ below the $N^+ = 5$ ionization threshold. The pulsed electric field

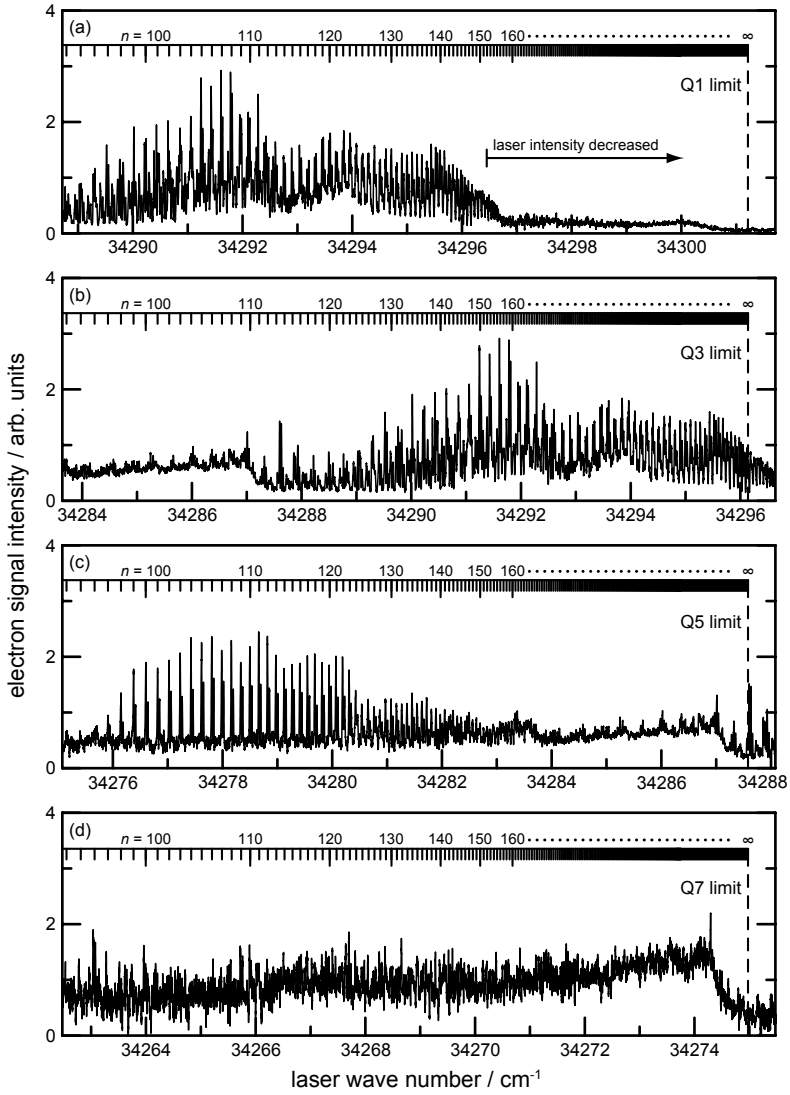

FIG. 4. RSR-TI spectra of $^4He_2$ recorded in regions (a) Q1, (b) Q3, (c) Q5, and (d) Q7 (see Fig. 2 for the definition of these regions).

leads to the ionization of the $24p7_N$ Rydberg states because it makes the $N^+ = 5$ ionization continuum energetically accessible and also because it facilitates rotational autoionization.[38]

No transitions to $N^+ = 5$ Rydberg states are observed in region O7 because the excitation efficiency from the initial $N'' = 7$ state is too low. The dominant Rydberg series are those with $N^+ = N''$ and transitions corresponding to $N^+ = N'' \pm 2, N'' \pm 4, \ldots$ make no significant contribution to the spectra (see discussion in Ref. 18). This situation is also encountered in np Rydberg series of H_2 (see, *e.g.*, Ref. 40) and N_2 (see, *e.g.*, Ref. 41) when excitation is from an initial orbital of dominant s character.[42]

The RSR-TI spectra recorded in regions Q1–Q7 are presented in Fig. 4. Transitions to

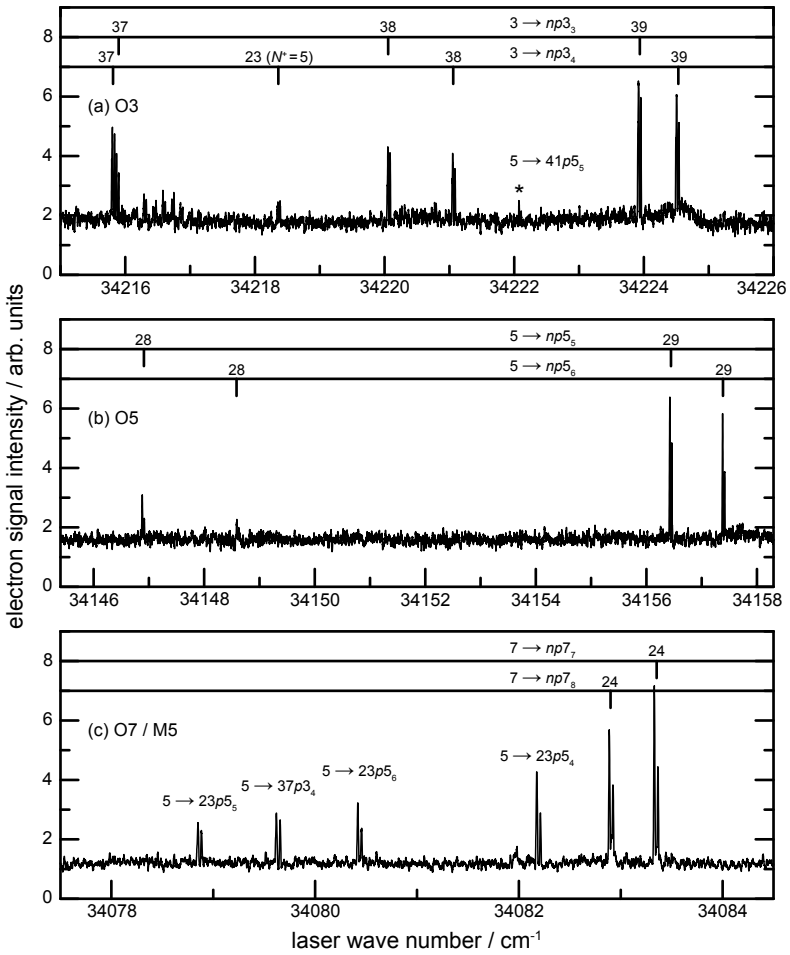

FIG. 5. RSR-TI spectra of $^4He_2$ recorded in regions (a) O3, (b) O5, and (c) O7 and M5 (see Fig. 2 for the definition of these regions). The line marked with an asterisk in panel (a) is affected by p-f interaction (see Section III F for discussion).

$np1_N$ Rydberg states are dominant in region Q1 and resolved in the range $n = 95$–145 (see assignment bars in Fig. 4a). Region Q3 is located only $4.9\,\mathrm{cm}^{-1}$ below region Q1 because the rotational constant of He_2^+ is slightly smaller than that of He_2^*.[18] The RSR-TI spectrum recorded in region Q3 is depicted in Fig. 4b and overlaps with regions Q1 and Q5. No regular series of lines converging to the Q3 ionization limit is visible in the spectrum, presumably because the lifetime of the $np3_N$ Rydberg states around $n = 100$ is shorter than $2\,\mu$s. The decay mechanism is rapid rotational autoionization into the $N^+ = 1$ continuum for the $N = 2$ levels and rotational autoionization induced by the p-f interaction and by the stray electric field for the $N = 3, 4$ levels, as explained in Section III F. In region Q5, on the other hand, a regular Rydberg series is observed (see Fig. 4c), which can be assigned to the $np5_6$ Rydberg series on the basis of the calculations presented in Ref. 18. The spectrum recorded in region

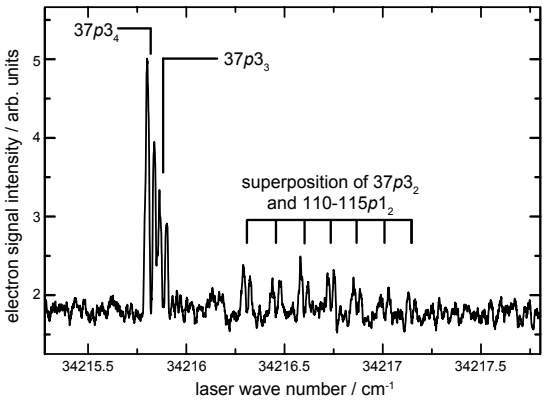

FIG. 6. Enlarged view of the observed RSR-TI spectrum in region O3 near the $3 \rightarrow 37p3_N$ transitions.

Q7, presented in Fig. 4d, does not reveal any clearly resolved Rydberg series converging to the $N^+ = 7$ ionization threshold. The $np7_N$ Rydberg states with $n < 150$ autoionize before the electric-field pulse is applied and are therefore not detected. For $n > 150$, the signal of the unresolved $np7_N$ Rydberg series gradually increases up $34\,274.3\,\mathrm{cm}^{-1}$, which corresponds to the position where the $n \approx 400$ Rydberg states are expected. This increase is attributed to the increase of the lifetime with growing n values and is consistent with the fact that the autoionization lifetimes of Rydberg states scale as n^{4-5} in the presence of stray electric fields.[43,44] Rydberg states with $n > 400$ are not stable in the presence of the stray electric field of $\sim 0.01\,\mathrm{V/cm}$.

The RSR-TI spectra recorded in the regions O3–O7 and M5 are presented in Fig. 5. In these regions, the sharp structures correspond to transitions to Rydberg states that are detected following field-induced rotational autoionization. In the spectrum recorded in region O3 (see Fig. 5a), two Rydberg series, the $3 \rightarrow np3_3$ and $3 \rightarrow np3_4$ series, are visible, as indicated by the assignment bars. Whereas the $np3_3$ Rydberg series is regular, the members of the $np3_4$ series between $n = 37$ and $n = 39$ are strongly perturbed by a rotational channel interaction with the $23p5_4$ Rydberg state. The rotational channel interaction leads to pronounced level shifts which are quantitatively analyzed in Section III C. Members of two Rydberg series are also observed in the O5 and O7 regions, as illustrated in Fig. 5b and 5c, respectively. The O7 and M5 regions overlap and the four lowest transitions observed in Fig. 5c are assigned to M5 transitions on the basis of their fine structure (see Section III B).

The assignment of the line marked with an asterisk in Fig. 5a is discussed in Section III F. An additional spectral structure, displayed on an enlarged scale in Fig. 6, is observed near

TABLE II. Term values and fine-structure splittings of the ($v'' = 0, N'' = 1$–7) rovibrational levels of the $2s\sigma\, a\,^3\Sigma_u^+$ metastable state of $^4He_2$ taken from Ref. 28. All values are given in units of cm^{-1}.

N''	$\tilde{\nu}_{obs}$ [a]	F_1 [b]	F_2 [b]	F_3 [b]
1	15.1760(1)	0.0049	−0.0243	0.0491
3	90.9889(3)	0.0079	−0.0243	0.0199
5	227.1697(8)	0.0089	−0.0242	0.0167
7	423.2366(16)	0.0094	−0.0241	0.0155

[a] Term values relative to the hypothetical ($v'' = 0, N'' = 0$) level of the $2s\sigma\, a\,^3\Sigma_u^+$ state and corresponding to the center of gravity of the three fine-structure components.

[b] Splittings resulting from the spin fine structure. F_1, F_2, and F_3 denote the fine-structure components with $J'' = N'' + 1, J'' = N''$, and $J'' = N'' - 1$, respectively.

34 217 cm^{-1} in region O3 of the RSR-TI spectrum. The four strong lines on the left-hand side of Fig. 6 correspond to the $N = 3$ and $N = 4$ orbital fine-structure components of the $37p3_N$ Rydberg state. The weaker set of lines located in the center of Fig. 6 appears at the position where the $37p3_2$ Rydberg state is expected. This state is not observed as a single resonance because of the rotational channel interaction with members of the $np1_2$ Rydberg series around $n = 112$ which gain intensity from the strong $37p3_2$ transition. The splitting observed for all transitions in Fig. 6 originates from the fine structure of the $N'' = 3$ initial state, as discussed in the next section.

B. Determination of term values

The term values of the levels reported in this article correspond to their wave numbers relative to the hypothetical ($v'' = 0, N'' = 0$) level of the $2s\sigma\, a\,^3\Sigma_u^+$ metastable state of He_2. The term values of the rotational levels of the metastable state are known accurately from high-resolution near-infrared emission spectroscopy[28] and are listed in the second column of Table II. Each of these rotational levels is split into three components labeled F_1 (for $J'' = N'' + 1$), F_2 (for $J'' = N''$), and F_3 (for $J'' = N'' - 1$) by the spin-spin and spin-rotation interactions. The spin fine structure reported in Ref. 28 is included in Table II.

The term values of triplet np Rydberg states of He_2 were determined from the spectra presented in the previous section by adding the observed transition wave numbers to the term values of the initial metastable states given in Table II. The spin fine structure of the metastable states, which was partially resolved in the measurements (see, *e.g.*, Fig. 3), had

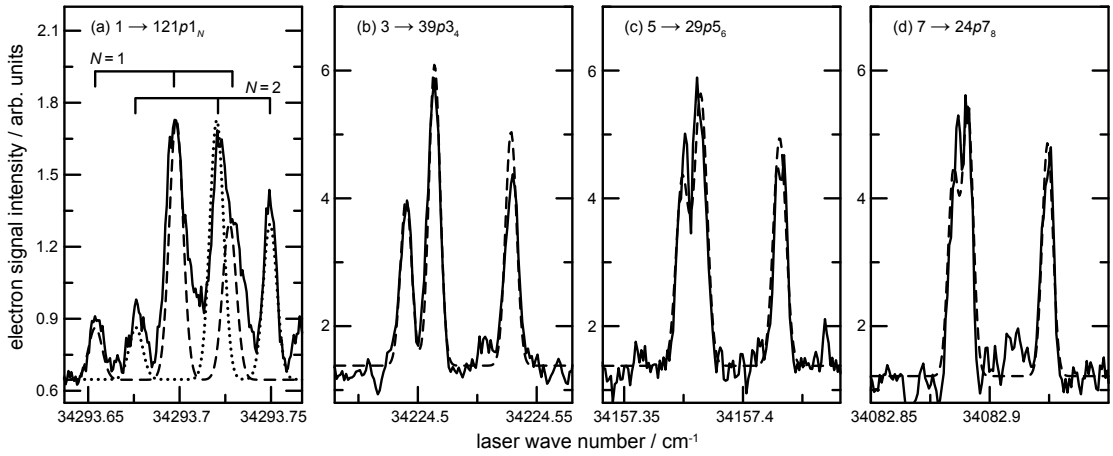

FIG. 7. Enlarged view of the observed RSR-TI spectra around selected transitions (solid lines). The dashed and dotted lines represent the simulated lineshapes (see text for details).

to be taken into account in the lineshape model in order to extract reliable experimental transition wave numbers. The spin fine structure of the final triplet np Rydberg states, which is expected to scale as n^{-3}, could not be resolved and was neglected in the analysis. For each transition, four fit parameters were used to model the observed lineshape: the wave number corresponding to the center of gravity of the transition, the linewidth, a constant background signal, and the intensity of the central (F_1) spin fine-structure component. The intensity ratio between the F_1, F_2, and F_3 components was fixed to the ratio expected from the degeneracy factor $2J'' + 1$. Representative fits of the lineshape model to observed intensity distributions of transitions originating from metastable levels with $N'' \leq 7$ are presented in Fig. 7. For the $1 \rightarrow np1_N$ transitions, which were observed only for $n > 86$, the $N = 1$ and $N = 2$ orbital fine-structure components partially overlap and were therefore fitted simultaneously, as illustrated in Fig. 7a for the $1 \rightarrow 121p1_N$ transitions. The dashed and dotted lines in Fig. 7a represent the simulated contributions of the $N = 1$ and $N = 2$ orbital fine-structure components, respectively. The N'' dependence of the fine structure observable in Fig. 7 turned out to be very useful in the analysis because it enabled the unambiguous assignment of the N'' quantum number. All assignments presented in the previous section were confirmed in this way.

The experimental term values of all triplet np Rydberg states observed in the RSR-TI spectra recorded in regions Q1–Q7 are listed in Table III. The $N = 1$ and $N = 2$ Rydberg series converging to the $N^+ = 1$ threshold have approximately the same intensity

TABLE III. Experimental term values of triplet np Rydberg states of $^4He_2$ observed in the RSR-TI spectra recorded in the regions Q1–Q7 (see Fig. 4) and comparison with the results of MQDT calculations. All values are given in units of cm^{-1}.

	$np1_1$ series		$np1_2$ series		$np3_4$ series		$np5_6$ series	
n	$\tilde{\nu}_{obs}$	o–c[a]	$\tilde{\nu}_{obs}$	o–c[a]	$\tilde{\nu}_{obs}$	o–c[a]	$\tilde{\nu}_{obs}$	o–c[a]
87	34301.8616	−0.0005	34301.8776	0.0004				
88	34302.1901	−0.0004	34302.1952	−0.0002				
89	34302.5074	−0.0004	34302.4985	0.0001				
90	34302.8145	−0.0003	34302.7814	−0.0005				
91	34303.1109	−0.0007	34303.0385	0.0004				
92	34303.3980	−0.0007	34303.2689	−0.0010				
93	34303.6763	−0.0004	34303.7537	0.0012				
94	34303.9456	−0.0002	34304.0059	0.0011				
95	34304.2064	−0.0000	34304.2539	−0.0011	34375.1054	−0.0012		
96	34304.4588	−0.0002			34375.3437	−0.0002		
97	34304.7023	−0.0014	34304.7396	0.0001	34375.5699	−0.0011		
98	34304.9412	0.0002	34304.9736	0.0013	34375.7892	−0.0004	34503.3314	−0.0010
99	34305.1709	−0.0003	34305.1993	0.0007	34376.0032	0.0005	34503.5596	−0.0014
100	34305.3933	−0.0012	34305.4193	0.0008	34376.2117	−0.0008	34503.7828	0.0001
101	34305.6109	−0.0002	34305.6328	0.0007			34503.9974	−0.0005
102	34305.8213	−0.0002	34305.8383	−0.0012			34504.2073	0.0005
103	34306.0248	−0.0009	34306.0406	−0.0003			34504.4101	0.0004
104	34306.2229	−0.0011	34306.2370	0.0004	34377.2143	0.0002	34504.6066	0.0001
105	34306.4166	−0.0002	34306.4265	0.0007	34377.4017	−0.0002	34504.7988	−0.0007
106	34306.6037	−0.0003	34306.6115	0.0018	34377.5853	0.0001	34504.9846	0.0005
107	34306.7875[b]	0.0014	34306.7875[b]	−0.0003	34377.7647	0.0009	34505.1656	0.0006
108	34306.9616[b]	−0.0015	34306.9616[b]	0.0017	34377.9385	0.0007	34505.3411	0.0003
109	34307.1361	0.0006	34307.1264	0.0002	34378.1087	0.0013	34505.5125	0.0007
110	34307.3025	−0.0003	34307.2846	−0.0005			34505.6788	0.0006
111	34307.4656	−0.0002	34307.4345	−0.0013			34505.8412	0.0011
112	34307.6241	−0.0003	34307.5770	−0.0007			34505.9999	0.0023
113	34307.7794	0.0006	34307.7131	0.0001			34506.1532	0.0023
114	34307.9283	−0.0009					34506.3029	0.0026
115	34308.0759	0.0002	34308.1183	−0.0005			34506.4485	0.0028
116	34308.2183	−0.0001	34308.2562	0.0017			34506.5899	0.0026
117	34308.3576	0.0002	34308.3889	0.0002			34506.7291	0.0038
118	34308.4925	−0.0005	34308.5212	0.0007			34506.8634	0.0037
119	34308.6246	−0.0005	34308.6505	0.0008			34506.9954	0.0046
120	34308.7541	0.0002	34308.7775	0.0013			34507.1238	0.0053
121	34308.8790	−0.0006	34308.9012	0.0014			34507.2484	0.0053
122	34309.0021	−0.0001	34309.0228	0.0021			34507.3698	0.0053
123	34309.1232	0.0015	34309.1405	0.0016			34507.4890	0.0062
124	34309.2394	0.0009	34309.2564	0.0021			34507.6073	0.0047
125	34309.3524	0.0000	34309.3692	0.0022			34507.7217	0.0105
126	34309.4647	0.0011	34309.4794	0.0023				

[a] Difference between observed term values and term values calculated using the eigenquantum defects from Table VI and the adjusted rovibrational energies of $^4He_2^+$ (see Table VIII).

[b] The $N = 1$ and 2 orbital fine-structure components of the $n = 107$ and 108 states could not be resolved.

TABLE IV. Experimental term values of triplet np Rydberg states of $^4He_2$ observed in regions O3–O7 and M5 (see Fig. 5) and comparison with the results of MQDT calculations. All values are given in units of cm^{-1}.

Label	$\tilde{\nu}_{obs}$	o–c[a]	Label	$\tilde{\nu}_{obs}$	o–c[a]
Negative electronic parity			Positive electronic parity		
$37p3_3$	34306.8625	−0.0039	$37p3_4$	34306.7999	0.0068
			$23p5_4$	34309.3555	−0.0030
$38p3_3$	34311.0502	−0.0027	$38p3_4$	34312.0515	−0.0037
$39p3_3$	34314.9179	−0.0031	$39p3_4$	34315.5038	−0.0024
$23p5_5$	34306.0302	0.0031	$23p5_6$	34307.6006	0.0090
$28p5_5$	34374.0618	0.0009	$28p5_6$	34375.7730	0.0020
$29p5_5$	34383.6051	−0.0007	$29p5_6$	34384.5609	0.0019
$24p7_7$	34506.5783	0.0056	$24p7_8$	34506.1368	0.0082
root-mean-square:		0.0033	root-mean-square:		0.0054

[a] Difference between observed term values and term values calculated using the eigenquantum defects from Table VI. The rovibrational energy levels and potential-energy curve of $^4He_2^+$ in the $X^+\,^2\Sigma_u^+$ ground state were taken from recent *ab initio* calculations.[7]

(see Fig. 7a), except near the $96p1_2$ and $114p1_2$ Rydberg states, where the intensity of the $N = 2$ series is reduced because of rotational channel interactions with members of the $np3_2$ series. No members of Rydberg series with $N = N^+ - 1$ were observed in regions Q3-Q7, presumably because they are subject to fast rotational autoionization. In regions Q3 and Q5 of the RSR-TI spectrum, only transitions to the $N = N^+ + 1$ orbital fine-structure components were observed and transitions to the $np3_4$ Rydberg states appear much weaker than transitions to the $np5_6$ Rydberg states. These observations can be explained by the autoionization lifetimes of the final Rydberg states (see Section III F below).

The term values of np Rydberg states observed in regions O3–O7 and M5 are listed in Table IV. The $37p3_4$ and $23p5_4$ Rydberg states were observed from the $N'' = 3$ and $N'' = 5$ levels of the metastable state (see panels a and c of Fig. 5). The term values determined from these transitions differ by less than $0.004\,cm^{-1}$, which is within the estimated accuracy of the wave-number calibration (see Table I).

C. Adjustment of eigenquantum-defect parameters

To analyze the spectra, we used MQDT as developed by Ch. Jungen and his coworkers.[40,45–54] MQDT using η eigenquantum defects[47–49,54] was applied to quantitatively describe the ob-

served term values of triplet np and nf Rydberg states of He_2 converging to the $X^+\,^2\Sigma_u^+$ ground state of He_2^+. MQDT describes these states in terms of eigenquantum-defect functions $\eta_{\ell\ell'}^{(\Lambda)}(R,\varepsilon)$, where R is the internuclear distance and ε is the energy of the Rydberg electron divided by the Rydberg constant:

$$\varepsilon = \frac{E - E^+}{hc\mathcal{R}_{\mathrm{He_2}}}. \tag{2}$$

In Eq. (2), E is the total energy and E^+ is the energy of the $^4He_2^+$ ion core in the $X^+\,^2\Sigma_u^+$ ground state taken from recent *ab initio* calculations.[7] The procedure and the program, developed by Ch. Jungen and his coworkers[40,45–54], to calculate Rydberg spectra from the eigenquantum-defect functions were the same as used in a recent study of the triplet ns and nd Rydberg states of H_2.[55] In that study, the eigenquantum-defect parameters of H_2 were extracted from available *ab initio* potential-energy curves[56–59] and subsequently adjusted to fit experimental data. No highly accurate potential-energy curves are available for the lowest Rydberg states of He_2 and eigenquantum-defect parameters had to be obtained directly in a fit to experimental term values of triplet np and nf Rydberg states. As in Ref. 55, the fitting procedure was divided into two steps. In the first step (fit A), the $\eta_{pp}^{(\Pi)}$, $\eta_{pf}^{(\Pi)}$, $\eta_{ff}^{(\Pi)}$, $\eta_{ff}^{(\Delta)}$, and $\eta_{ff}^{(\Phi)}$ eigenquantum defects were determined and only Rydberg states of negative electronic parity were considered, *i.e.*, the $np\,^3\Pi_g^-$, $nf\,^3\Pi_g^-$, $nf\,^3\Delta_g^-$, and $nf\,^3\Phi_g^-$ states when using Hund's-case-(b) notation, or the npN_N^+ and nfN_N^+ Rydberg states with even values of $N^+ - N$ when using Hund's-case-(d) notation. The reason for a separate fit of levels with negative electronic parity is that the positions of these levels do not depend on eigenquantum-defect parameters of Σ symmetry. The $\eta_{pp}^{(\Sigma)}$, $\eta_{pf}^{(\Sigma)}$, and $\eta_{ff}^{(\Sigma)}$ eigenquantum defects were then adjusted in the second step (fit B) to reproduce the observed positions of the energy levels with positive electronic parity.

The eigenquantum-defect functions of He_2 were determined by adjusting their values at predefined values of R and ε, *i.e.*, $R = 1.8\,a_0, 2.1\,a_0, 2.4\,a_0$ and $\varepsilon = 0, {}^{-1}\!/_{4^2}, {}^{-1}\!/_{3^2}$ for the $\eta_{pp}^{(\Pi)}$ eigenquantum defects adjusted in fit A. The values $\varepsilon = 0, {}^{-1}\!/_{4^2}, {}^{-1}\!/_{3^2}$ correspond to states with $n \to \infty$, $n = 4$, and $n = 3$, respectively. The values of $\eta_{pp}^{(\Pi)}(R,\varepsilon)$ at arbitrary values of (R,ε) were obtained by extrapolation using polynomial functions which are quadratic in R and ε. The $\eta_{pf}^{(\Pi)}$, $\eta_{ff}^{(\Pi)}$, $\eta_{ff}^{(\Delta)}$, and $\eta_{ff}^{(\Phi)}$ eigenquantum defects were also adjusted in fit A, but were assumed to be independent of R and linearly dependent on ε. In addition to

TABLE V. Experimental term values of triplet np and nf Rydberg states of $^4He_2$ with $n = 4$ and 5 taken from the literature[22,27,29] and comparison with the results of MQDT calculations. All values are given in units of cm^{-1}.

	$4p\pi\,^3\Pi_g\,(v=0)$[22]			$4f\,(v^+=0)$[27]				$5p\pi\,^3\Pi_g\,(v=0)$[22]			$5f\,(v^+=0)$[29]			
N	$\tilde{\nu}_{\rm obs}$	o–c[a]	$\Delta\tilde{\nu}_{pf}$[b]	N^+	$\tilde{\nu}_{\rm obs}$	o–c[a]	$\Delta\tilde{\nu}_{pf}$[b]	$\tilde{\nu}_{\rm obs}$	o–c[a]	$\Delta\tilde{\nu}_{pf}$[b]	N^+	$\tilde{\nu}_{\rm obs}$	o–c[a]	$\Delta\tilde{\nu}_{pf}$[b]
Used in fit A (levels with negative electronic parity)														
1	27207.12	−0.04	−0.14	3	27492.24	0.01	0.12	29799.60	0.02	−0.08	3	29978.33	0.07	0.07
3	27278.36	−0.02	−0.16	1	27462.42	0.07	0.04	29870.63	−0.01	−0.11	1	29931.15	0.08	0.03
				3	27529.58	−0.01	0.04				3	29995.96	0.10	0.04
				5	27632.97	0.01	0.05							
5	27406.29	−0.03	−0.18	3	27526.41	0.05	0.08	29999.56	−0.00	1.12	3	29996.03[c]	−0.02	−1.19
				5	27659.77	−0.01	0.05				5	30125.96	0.16	0.04
				7	27820.57	−0.04	0.04				7	30297.68	−0.14	0.02
7	27590.42	−0.06	−0.26	5	27651.25	0.02	0.16	30182.21	−0.08	−0.01	5	30122.91	0.05	−0.05
											7	30309.60	−0.30	0.04
9	27828.41	0.00	−2.21	7	27835.08	−0.14	2.11	30421.57	−0.07	−0.03	7	30305.39	−0.03	−0.03
Used in fit B (levels with positive electronic parity)														
2	27234.64	−0.04	−0.17	1	27424.21	0.12	0.07	29826.56	0.05	−0.12	1	29909.44	−0.12	0.08
				3	27508.53	0.14	−0.02				3	29986.43	−0.24	−0.01
				5	27617.03	−0.07	−0.01				5	30104.17	−0.32	−0.01
4	27332.03	0.03	−0.25	1	27431.53	0.08	0.17	29923.38	0.02	0.68	1	29913.30	−0.05	−0.72
				3	27536.04	0.00	0.00				3	30000.85	0.04	0.01
				5	27648.75	0.05	−0.02				5	30120.83	0.72	−0.01
				7	27802.71	−0.23	−0.01							
6	27484.00	0.29	−1.25	3	27501.15	−0.15	1.18	30073.53	0.05	0.04	3	29983.01	−0.17	−0.09
				5	27661.49	0.02	0.01				5	30127.76	0.15	0.03
											7	30305.85	0.49	−0.01
8	27692.74	0.02	0.25	5	27626.23	0.01	−0.32	30278.68	0.08	0.00	5	30109.67	−0.22	−0.05
											7	30310.89	0.26	0.04

[a] Difference between observed term values and term values calculated using the eigenquantum defects from Table VI including the p-f interaction.
[b] Calculated shifts induced by the p-f interaction.
[c] The term value of the $5f3_5\,(v^+=0)$ Rydberg state was taken from Ref. 22.

these $9 + 4 \times 2 = 17$ fit parameters for the eigenquantum-defect functions, the position of the $N^+ = 1$ ionization threshold relative to the hypothetical $(v'' = 0, N'' = 0)$ level of the $2s\sigma\,a\,^3\Sigma_u^+$ state of He_2 was also adjusted during fit A, resulting in a total of 18 adjustable parameters.

In the subsequent fit (fit B), the final values of all 18 fit parameters determined in fit A were used without further adjustments and only the eigenquantum defects of Σ symmetry were adjusted. The 12 fit parameters used for the $\eta_{pp}^{(\Sigma)}$ eigenquantum defect are the values

at $R = 1.8\,a_0, 2.1\,a_0, 2.4\,a_0, 2.7\,a_0$ and $\varepsilon = 0, {}^{-1}/_{4^2}, {}^{-1}/_{3^2}$. The values of $\eta_{pp}^{(\Sigma)}(R,\varepsilon)$ at arbitrary values of (R,ε) were obtained by extrapolation using polynomial functions which are cubic in R and quadratic in ε. The $\eta_{ff}^{(\Sigma)}$ eigenquantum defect was assumed to be independent of R and linearly dependent on ε, and the $\eta_{pf}^{(\Sigma)}$ eigenquantum defect was assumed to be independent of R and ε. The total number of fit parameters adjusted in fit B was therefore $12 + 2 + 1 = 15$.

The experimental data set used in fit A consisted of 261 triplet np and nf Rydberg states with negative electronic parity, $v^+ \leq 2$, $N^+ \leq 19$, and n in the range 2–39. In fit B, 230 triplet np and nf Rydberg states with positive electronic parity, $v^+ \leq 2$, $N^+ \leq 9$, $N \leq 8$, and n in the range 2–39 were used. From the total of 491 energy levels, 15 triplet np levels were taken from Table IV above, 437 triplet np levels were taken from measurements carried out by Ginter and coworkers,[22–26] 19 triplet $4f$ levels were taken from Herzberg and Jungen,[27] and 20 triplet $5f$ levels were taken from Kawaguchi *et al.*[29] All term values of triplet np Rydberg states taken from the literature are provided in the supplementary material[60] and the term values of the $4f$ and $5f$ Rydberg states[27,29] are listed in Table V together with data on $4p\pi\,{}^3\Pi_g$ and $5p\pi\,{}^3\Pi_g$ Rydberg states.[22] The data extracted from the RSR-TI spectra recorded in regions Q1–Q7 (Table III) were not used, because high-n Rydberg states with $n > 86$ are not sensitive to adjustments of eigenquantum defects. These states, however, are sensitive to adjustments of the ionization energies and were used to extract rotational energy spacings in $^4\mathrm{He}_2^+$ (see Section III E below). All experimental data were weighted according to their uncertainty, which was assumed to be $0.006\,\mathrm{cm}^{-1}$ for the term values taken from Table IV and $0.1\,\mathrm{cm}^{-1}$ for all term values taken from the literature. The basis used in the MQDT calculations included np channels up to $v^+_{\mathrm{max}} = 7$ and nf channels up to $v^+_{\mathrm{max}} = 3$. An increase of the basis size did not lead to a change of the calculated term values, as was tested using the final eigenquantum-defect parameters.

The final values of all eigenquantum-defect parameters adjusted in fits A and B are given in Table VI and the final term value of the $N^+ = 1$ ionization threshold with respect to the Pauli-forbidden $(v'' = 0, N'' = 0)$ level of the $2s\sigma\,a\,{}^3\Sigma_u^+$ state was determined to be $34\,316.391\,\mathrm{cm}^{-1}$ (standard deviation $0.002\,\mathrm{cm}^{-1}$, absolute uncertainty $0.010\,\mathrm{cm}^{-1}$). The differences between the observed and calculated term values are listed next to the experimental term values in Table IV, Table V, and in the supplementary material.[60] The MQDT calculations reproduce the 15 triplet np Rydberg states given in Table IV with a root-mean-square

TABLE VI. Final values of the eigenquantum-defect parameters $\eta_{\ell\ell'}^{(\Lambda)}(R,\varepsilon)$ of He_2. The standard deviation in units of the last digit is given in parentheses.

$\ell\ell'$	Λ	R/a_0	$\varepsilon = 0$	$\varepsilon = -1/4^2$	$\varepsilon = -1/3^2$
From fit A (to levels with negative electronic parity)					
pp	Π	1.8	0.086 98(18)	0.092 36(7)	0.097 19(5)
pp	Π	2.1	0.069 62(3)	0.073 85(1)	0.077 76(1)
pp	Π	2.4	0.054 63(10)	0.057 94(4)	0.061 25(3)
pf	Π	2.1[a]	0.002 72(21)	0.001 76(4)	
ff	Π	2.1[a]	0.012 32(16)	0.010 75(3)	
ff	Δ	2.1[a]	0.004 09(20)	0.003 39(3)	
ff	Φ	2.1[a]	−0.007 62(20)	−0.008 58(4)	
From fit B (to levels with positive electronic parity)					
pp	Σ	1.8	−0.2405(14)	−0.2341(5)	−0.2294(8)
pp	Σ	2.1	−0.2240(2)	−0.2182(1)	−0.2128(1)
pp	Σ	2.4	−0.1973(7)	−0.1943(25)	−0.1894(4)
pp	Σ	2.7	−0.1332(19)	−0.1472(52)	−0.1499(8)
pf	Σ	2.1[a]	0.0022(3)[b]	0.0022(3)[b]	
ff	Σ	2.1[a]	0.0140(4)	0.01324(4)	

[a] All pf and ff eigenquantum defects were assumed to be R independent.
[b] The $\eta_{pf}^{(\Sigma)}$ eigenquantum defects were assumed to be energy independent.

(rms) deviation of $0.0045\,\mathrm{cm}^{-1}$. For the low-np and nf Rydberg states, the rms deviation amounts to $0.103\,\mathrm{cm}^{-1}$ for the levels with negative electronic parity and $0.197\,\mathrm{cm}^{-1}$ for the levels with positive electronic parity. Several levels of the $4p\pi\,{}^3\Pi_g$ and $5p\pi\,{}^3\Pi_g$ states are strongly perturbed by close-lying $4f$ and $5f$ Rydberg states *via* the p-f interaction, as was pointed out previously.[22,27,29] Our MQDT calculations accurately reproduce these perturbations as can be seen in Table V. The calculated shifts induced by the p-f interaction are also included in Table V and can be as large as $2.2\,\mathrm{cm}^{-1}$.

Because the quantum defect of the $np\sigma\,{}^3\Sigma_g^+$ states (~ -0.2) is very different from the quantum defect of the nf states (~ 0.0), the corresponding series are well separated. The p-f interaction does not induce significant shifts in low-n Rydberg states of Σ symmetry. The $\eta_{pf}^{(\Sigma)}$ eigenquantum-defect parameter is therefore poorly defined by the data set and we expect the uncertainty of its value listed in Table VI to be larger than the standard deviation.

The final triplet $\eta_{pp}^{(\Sigma)}(R,\varepsilon)$ and $\eta_{pp}^{(\Pi)}(R,\varepsilon)$ eigenquantum-defect functions of He_2 are displayed in Fig. 8. Their values at $R = 2.1\,a_0$ and $\varepsilon = 0$ are −0.2240(2) and 0.06962(3), respectively. Whereas the value of the $\eta_{pp}^{(\Pi)}$ eigenquantum defect lies between the values

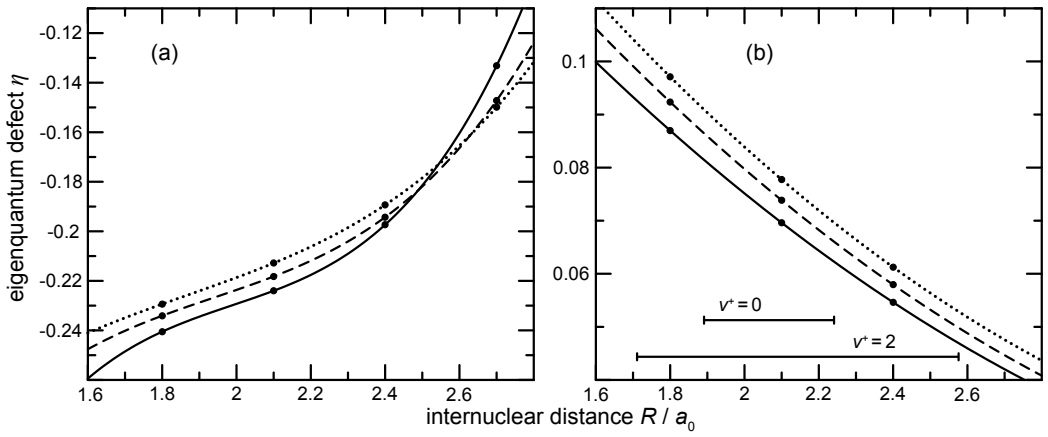

FIG. 8. (a) $\eta_{pp}^{(\Sigma)}(R,\varepsilon)$ and (b) $\eta_{pp}^{(\Pi)}(R,\varepsilon)$ eigenquantum-defect functions of He_2 after adjustment to experimental data at $\varepsilon = 0$ (solid lines), $\varepsilon = -1/4^2$ (dashed lines) and $\varepsilon = -1/3^2$ (dotted lines). The dots represent the fit parameters adjusted in fits A and B (see Table VI). The intervals given in panel (b) depict the classically allowed range of R values for He_2^+ in the states $(v^+ = 0, N^+ = 1)$ and $(v^+ = 2, N^+ = 1)$.

determined in Ref. 18 for the $v^+ = 0$ and $v^+ = 1$ Rydberg series, our $\eta_{pp}^{(\Sigma)}$ eigenquantum defect is lower by 1 than in Ref. 18. A shift by 1 does not change the resulting level energies, but changes the calculated rotational (N^+) character in the vicinity of rotational channel interactions. Such an interaction is encountered, *e.g.*, in the $np3_4$ Rydberg series around $n = 38$, as already discussed in Section III A in the context of Fig. 5 (see lower assignment bar in panel a). Using our *pp* eigenquantum defects, the second line assigned to the $N'' \rightarrow N = 4$ series and observed at $34\,218.4\,\mathrm{cm}^{-1}$ in Fig. 5a is calculated to have the largest $N^+ = 5$ character (73 %), which explains its weak intensity. When shifting the $\eta_{pp}^{(\Sigma)}$ eigenquantum defect by 1, the same member is calculated to have only 28 % $N^+ = 5$ character and 72 % $N^+ = 3$ character, whereas the first member of the series observed at $34\,215.8\,\mathrm{cm}^{-1}$ in Fig. 5a (labeled $37p3_4$) is calculated to have 75 % $N^+ = 5$ character, which agrees less well with the observed intensity distribution.

D. Determination of potential-energy curves of low-np Rydberg states of He_2

Potential-energy curves and eigenquantum-defect functions are closely related and can be transformed into each other.[45,47,48,50,53–55] The adjusted $\eta_{pp}^{(\Lambda)}(R,\varepsilon)$ eigenquantum-defect functions derived in the previous section were used to determine the potential-energy curves of the $np\sigma\,{}^3\Sigma_g^+$ and $np\pi\,{}^3\Pi_g$ Rydberg states of He_2 with $n \leq 5$ in the range of $R = 1.7$–$2.7\,a_0$.

TABLE VII. Born-Oppenheimer potential-energy curves $E_{\rm BO}$ of the lowest four $np\sigma\,{}^3\Sigma_g^+$ and $np\pi\,{}^3\Pi_g$ Rydberg states of He_2 (in units of the Hartree energy $E_{\rm h}$). The adiabatic corrections $E_{\rm ad}/hc$ are given in units of $\rm cm^{-1}$.

R/a_0	$E_{\rm BO}/E_{\rm h}$	$E_{\rm ad}/hc$	$E_{\rm BO}/E_{\rm h}$	$E_{\rm ad}/hc$	$E_{\rm BO}/E_{\rm h}$	$E_{\rm ad}/hc$	$E_{\rm BO}/E_{\rm h}$	$E_{\rm ad}/hc$
	$2p\sigma\,c\,{}^3\Sigma_g^+$		$3p\sigma\,{}^3\Sigma_g^+$		$4p\sigma\,{}^3\Sigma_g^+$		$5p\sigma\,{}^3\Sigma_g^+$	
1.7	−5.07995477	155.89	−5.02408949	155.05	−5.00379787	154.74	−4.99410549	154.60
1.8	−5.09099084	154.28	−5.03464699	153.44	−5.01426889	153.13	−5.00454093	152.98
1.9	−5.09743767	153.06	−5.04060425	152.20	−5.02013898	151.89	−5.01037865	151.75
2.0	−5.10048191	152.13	−5.04313911	151.26	−5.02258203	150.95	−5.01278966	150.81
2.1	−5.10105101	151.43	−5.04316926	150.56	−5.02251186	150.25	−5.01268491	150.10
2.2	−5.09986975	150.93	−5.04140876	150.05	−5.02063873	149.74	−5.01077181	149.59
2.3	−5.09750424	150.59	−5.03841179	149.70	−5.01751317	149.38	−5.00759800	149.24
2.4	−5.09439661	150.37	−5.03460687	149.47	−5.01356018	149.15	−5.00358565	149.00
2.5	−5.09089272	150.25	−5.03032369	149.34	−5.00910621	149.02	−4.99905845	148.87
2.6	−5.08726460	150.22	−5.02581421	149.29	−5.00440038	148.97	−4.99426279	148.82
2.7	−5.08372937	150.25	−5.02126928	149.31	−4.99963117	148.98	−4.98938459	148.83
	$2p\pi\,b\,{}^3\Pi_g$		$3p\pi\,{}^3\Pi_g$		$4p\pi\,{}^3\Pi_g$		$5p\pi\,{}^3\Pi_g$	
1.7	−5.11332824	156.39	−5.03505783	155.21	−5.00863856	154.81	−4.99664602	154.63
1.8	−5.12281618	154.76	−5.04518555	153.59	−5.01892001	153.20	−5.00698068	153.02
1.9	−5.12777641	153.51	−5.05073780	152.35	−5.02461724	151.96	−5.01272841	151.78
2.0	−5.12937152	152.56	−5.05288012	151.41	−5.02689610	151.02	−5.01505511	150.84
2.1	−5.12850453	151.85	−5.05251802	150.70	−5.02666237	150.31	−5.01486662	150.14
2.2	−5.12587528	151.32	−5.05035346	150.19	−5.02461828	149.80	−5.01286521	149.62
2.3	−5.12202417	150.96	−5.04692868	149.83	−5.02130626	149.44	−5.00959338	149.27
2.4	−5.11736640	150.71	−5.04266040	149.59	−5.01714323	149.21	−5.00546810	149.03
2.5	−5.11221888	150.57	−5.03786685	149.46	−5.01244761	149.07	−5.00080779	148.90
2.6	−5.10682138	150.51	−5.03278891	149.40	−5.00746041	149.02	−4.99585355	148.84
2.7	−5.10135333	150.51	−5.02760692	149.40	−5.00236213	149.02	−4.99078589	148.85

The p-f interaction was neglected and the one-channel quantization condition[47]

$$\frac{\tan \pi \sqrt{-1/\varepsilon}}{A_{\ell=1}(\varepsilon)} + \tan \pi \eta_{pp}^{(\Lambda)}(R,\varepsilon) = 0 \tag{3}$$

was solved for ε at fixed values of R. In Eq. (3), $A_{\ell=1}(\varepsilon) = 1 - \varepsilon^2$ is Ham's scaling factor.[48] From the solutions $\varepsilon(R)$ of Eq. (3), the Born-Oppenheimer energies $E_{\rm BO}$ were obtained using

$$E_{\rm BO}(R) = \varepsilon(R) \times hc\mathcal{R}_\infty + E_{\rm BO}^+(R), \tag{4}$$

where $\mathcal{R}_\infty$ is the Rydberg constant for infinite mass and $E^+_{\rm BO}(R)$ is the Born-Oppenheimer potential-energy curve of the $X^+\,^2\Sigma^+_u$ ground state of He_2^+. In Table VII, the resulting values of $E_{\rm BO}(R)$ are listed for the lowest four $np\sigma\,^3\Sigma^+_g$ and $np\pi\,^3\Pi_g$ Rydberg states of He_2 using the values of $E^+_{\rm BO}(R)$ from Ref. 7.

The adiabatic corrections to the Born-Oppenheimer potential-energy curves were estimated from the solutions $\varepsilon(R)$ of Eq. (3) using

$$E_{\rm ad}(R) = \varepsilon(R) \times hc(\mathcal{R}_{\rm He_2} - \mathcal{R}_\infty) + E^+_{\rm ad}(R). \tag{5}$$

The first term in Eq. (5) is the adiabatic correction originating from the Rydberg electron and $E^+_{\rm ad}(R)$ represent the adiabatic correction to the Born-Oppenheimer potential-energy curve of the $X^+\,^2\Sigma^+_u$ ground state of $^4He_2^+$ taken from the supplementary material presented in Ref. 7. The values of $E_{\rm ad}(R)$ are given in Table VII. The contributions to the adiabatic correction from the Rydberg electron are listed in the supplementary material[60] and only represent a small fraction of the overall adiabatic correction.

The effect of the p-f interaction on the Born-Oppenheimer potential-energy curves was investigated by solving the corresponding two-channel eigenvalue equation. The potential-energy curves of np and nf states do not cross and the shift of the electronic energies induced by the p-f interaction was found to be less than $0.1\,{\rm cm}^{-1}$, *i.e.*, smaller than the expected accuracy of the potential-energy curves presented in Table VII.

E. Determination of rotational term values in the $X^+\,^2\Sigma^+_u\,(v^+ = 0)$ ground state of $^4He_2^+$

The eigenquantum defects determined in Section III C are accurate to better than 0.002 (see Table VI), which allows the prediction of electron binding energies of high-n Rydberg states around $n = 100$ with an estimated accuracy of better than $0.0005\,{\rm cm}^{-1}$. MQDT can therefore be used to extrapolate the energies of the Rydberg states observed in regions Q1–Q5 of the RSR-TI spectra to their limits with high precision. The extrapolation was carried out simultaneously for all observed Rydberg series in a global fitting procedure (referred to as fit C hereafter). The three fit parameters adjusted in fit C were the term value of the $(v^+ = 0, N^+ = 1)$ ionization threshold and the positions of the $N^+ = 3$ and $N^+ = 5$

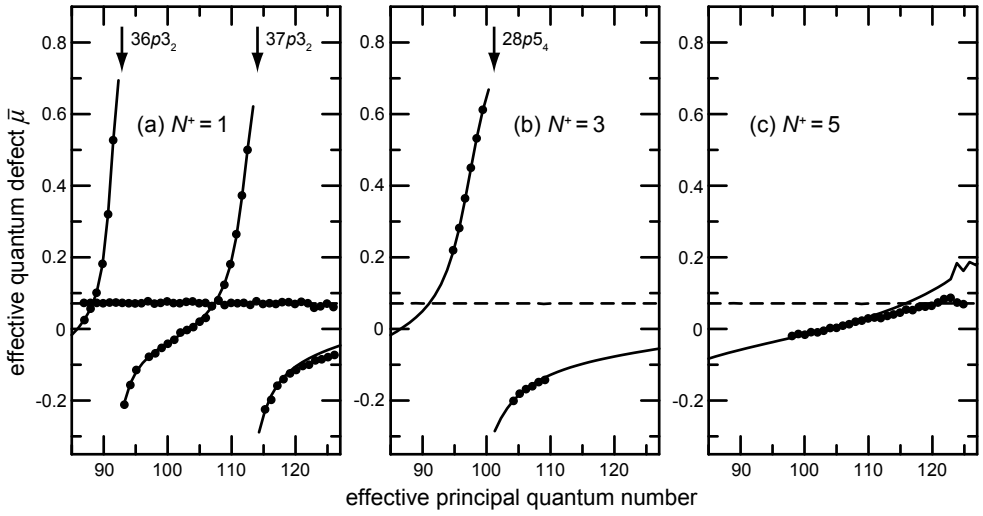

FIG. 9. Experimental (dots) and calculated (lines) quantum-defect plots of triplet np Rydberg states converging to the (a) $N^+ = 1$, (b) $N^+ = 3$, and (c) $N^+ = 5$ ionization thresholds of $^4He_2^+$ in the $X^+\,^2\Sigma_u^+$ ($v^+ = 0$) ground state. Solid and dashed lines depict the calculated effective quantum defects for the Rydberg series with $N = N^+ + 1$ and $N = N^+$, respectively.

levels of $^4He_2^+$ in the $X^+\,^2\Sigma_u^+$ ($v^+ = 0$) ground state relative to the $N^+ = 1$ level. Further rovibrational energies of $^4He_2^+$ used in the calculations were held fixed at their *ab initio* values from Ref. 7.

The experimental data set used in fit C consisted of 72 triplet np Rydberg states with $n \leq 110$ listed in Table III. Rydberg states with $n > 110$ were not included because their positions are more susceptible to stray electric fields. The same weight was given to all levels used in fit C.

The positions of the $N^+ = 3$ and $N^+ = 5$ rotational levels of $^4He_2^+$ in the $X^+\,^2\Sigma_u^+$ ($v^+ = 0$) ground state relative to the $N^+ = 1$ level resulting from fit C are $70.9372\,\mathrm{cm}^{-1}$ (standard deviation $0.0003\,\mathrm{cm}^{-1}$, absolute uncertainty $0.003\,\mathrm{cm}^{-1}$) and $198.3691\,\mathrm{cm}^{-1}$ (standard deviation $0.0003\,\mathrm{cm}^{-1}$, absolute uncertainty $0.006\,\mathrm{cm}^{-1}$), respectively. The term value of the ($v^+ = 0, N^+ = 1$) ionization threshold was $34\,316.3831\,\mathrm{cm}^{-1}$ (standard deviation $0.0001\,\mathrm{cm}^{-1}$, absolute uncertainty $0.010\,\mathrm{cm}^{-1}$). The difference between observed and calculated term values for all Rydberg states observed in regions Q1–Q5 of the RSR-TI spectra are included in Table III. The rms deviation of all $n \leq 110$ Rydberg states used in fit C is $0.0008\,\mathrm{cm}^{-1}$.

The observed and calculated positions of the high-n Rydberg states listed in Table III were transformed into effective quantum defects $\bar{\mu}$ using the Rydberg formula [Eq. (1)] and

are depicted in Fig. 9 as dots and lines, respectively. Rydberg series with $N = N^+$ are not affected by rotational channel interactions and their effective quantum defect is constant (see dashed lines in Fig. 9). Strong perturbations are visible for Rydberg series with $N = N^+ + 1$ at the positions of Rydberg states belonging to series converging to the $N^+ + 2$ ionization thresholds (indicated by vertical arrows). MQDT reproduces these perturbations within the experimental accuracy. Significant deviations are only present at large n values ($n > 120$ in Fig. 9a and $n > 110$ in Fig. 9c), presumably because of dc Stark shifts induced by the stray electric field.

F. Autoionization dynamics

In the absence of electric fields and when spins are ignored, the angular-momentum quantum number N of the Rydberg states of He_2 investigated here is conserved. For the $npN^+_{N=N^+-1}$ Rydberg states that are located energetically above the ionization thresholds associated with the $N^+ - 2$ ionic levels, rotational autoionization takes place on the sub-ns time scale up to n values beyond 100. These states are difficult to observe in the PI spectra because their natural linewidths are much larger than the laser linewidth, even at $n = 100$. They are typically not observed in the RSR-TI spectra either, because autoionization is complete long before the application of the delayed pulsed electric field used for field ionization and electron extraction. Members of the $npN^+_{N=N^+-1}$ Rydberg series located immediately below the $N^+ - 2$ ionization thresholds, however, are readily observed through their interactions with the long-lived high $npN^+{-}2_{N=N^+-1}$ Rydberg states (see, for example, Fig. 6).

The $npN^+_{N=N^+}$ and the $npN^+_{N=N^++1}$ Rydberg states cannot autoionize to p continua associated with the $N^+ - 2$ ionic levels, but can autoionize to $\ell = 3$ continua above the $N^+ - 2$ ionization threshold, the autoionization being mediated by the p-f interaction. The corresponding decay processes are slower than for the $npN^+_{N=N^+-1}$ Rydberg states, but still, in general, too fast for the corresponding series to be observed by delayed ($2\,\mu$s) pulsed field ionization. Fig. 4d, for instance, indicates that the lifetimes of the $np7_{7,8}$ Rydberg states are less than $1\,\mu$s up to $n = 100$. The Doppler-limited linewidth of the $24p7_{7,8}$ resonances in Fig. 5 suggests, however, that their lifetimes is at least about 1 ns at $n = 25$ and thus at least about 100 ns at $n = 100$ because of the n^3 scaling of the lifetimes.

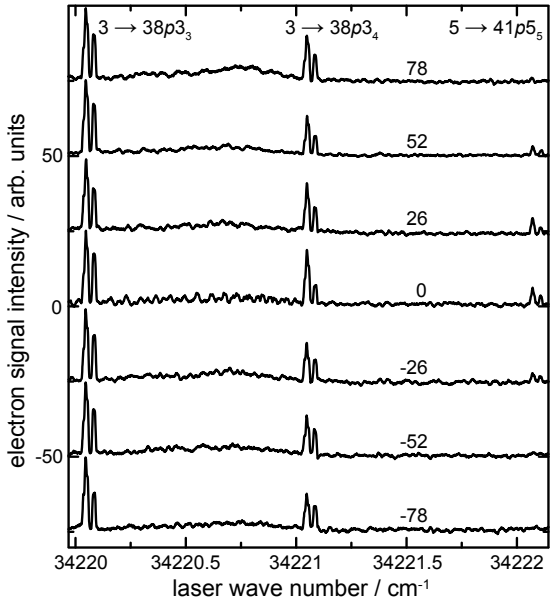

FIG. 10. RSR-TI spectra of $^4He_2$ recorded in the presence of different dc electric fields (shifted along vertical axis for clarity). The value of the applied dc electric field is given for each spectrum in units of mV/cm.

The line marked by an asterisk in Fig. 5a, and which is assigned to the $5 \rightarrow 41p5_5$ transition represents an exception. The $41p5_5$ Rydberg state is located above the O5 ionization threshold at $34\,160.15\,\mathrm{cm}^{-1}$ and is thus embedded in the $N^+ = 3$ ionization continua. The observation of this line in the RSR-TI spectrum is only possible if the lifetime of the $41p5_5$ Rydberg state is on the order of $1\,\mu$s or longer. No other members of the $np5_5$ Rydberg series with $n \leq 90$ and lying above the $N^+ = 3$ ionization threshold were observed in the RSR-TI spectra, indicating that their autoionization lifetimes are all much shorter than $1\,\mu$s, as a result of p-f-interaction-mediated autoionization. The explanation for the abnormally long lifetime of the $41p5_5$ Rydberg state is that it is almost degenerate with the $23f7_5$ Rydberg state (calculated to lie only $0.0508\,\mathrm{cm}^{-1}$ below the $41p5_5$ Rydberg state). As a result of this near-degeneracy, the p-f interaction induces a strong admixture of $f7_5$ character, which stabilizes the $41p5_5$ Rydberg state. The $nf7_5$ Rydberg states in this region are long lived because rotational autoionization would necessitate a change of core rotational quantum number of -4 and is hindered.[38]

The electric-field dependence of the RSR-TI spectrum recorded near the $5 \rightarrow 41p5_5$ and $3 \rightarrow 38p3_N$ transitions is depicted in Fig. 10. Whereas the intensities of the $3 \rightarrow 38p3_{3,4}$ transitions do not vary as a function of the dc electric field, the line corresponding to the

$5 \rightarrow 41p5_5$ transition disappears when dc electric fields larger than 52 mV/cm are applied. This observation can be explained by ℓ and N mixing induced by the field. The largest field-induced interactions affecting the $41p5_5$ Rydberg state are those with $\Delta\ell = \pm 1$ and $\Delta N = 0$ and autoionization is therefore expected to take place into the $d3_5$ continuum. The interaction, and thus the autoionization rate, increases gradually with the magnitude of the electric field, which eventually leads to the disappearance of the $5 \rightarrow 41p5_5$ transition in the spectra recorded when fields of ± 78 mV/cm are applied. These results indicate that the p-f interaction is not the sole mechanism responsible for the autoionization lifetimes of the $npN^+_{N=N^+}$ and the $npN^+_{N=N^++1}$ Rydberg series and that electric fields can also play an important role.

The measurement presented in Fig. 10 also allowed us to estimate the stray electric field in the excitation region: The intensity of the $5 \rightarrow 41p5_5$ transition measured when applying an electric field of -26 mV/cm is smaller than when an electric field of $+26$ mV/cm is applied, but corresponds approximately to the intensity measured when an electric field of $+52$ mV/cm is applied. We therefore conclude that a dc electric field of ~ 13 mV/cm is required to compensate the stray electric field (-13 mV/cm) present during laser excitation.

The joint effects of the p-f interaction and ℓ mixing by electric fields on the autoionization dynamics of the triplet np Rydberg states around $n = 100$ are illustrated by Fig. 11, which compares the PI and RSR-TI spectra recorded in regions Q3 and Q5 (see Fig. 2). The $np3_2$ and $np5_4$ series are not observed in these spectra because of rapid autoionization, as explained above. The calculated positions of the $np3_3$ and $np5_5$, the autoionization of which must be to an f continuum in the absence of fields, are indicated as vertical dotted lines in Figs. 11a and b, respectively. Transitions to these states are strong in the PI spectra, but absent from the RSR-TI spectra, confirming the observation made for the $np7_7$ series (see Fig. 4d) that the $npN^+_{N=N^+}$ series have lifetimes significantly shorter than 2 μs around $n = 100$. The calculated positions of the $npN^+_{N=N^++1}$ Rydberg series are indicated by vertical dashed lines in Fig. 11. Whereas the transitions to the $np3_4$ and $np5_6$ Rydberg states have approximately the same intensities in the PI spectra, the lines corresponding to the transitions to the $np3_4$ Rydberg states are four times weaker in the RSR-TI spectra than those corresponding to the $np5_6$ Rydberg states.

These observations suggest that the $npN^+_{N=N^++1}$ Rydberg states are longer lived than the $npN^+_{N=N^+}$ Rydberg states of the same principal quantum number. This difference may

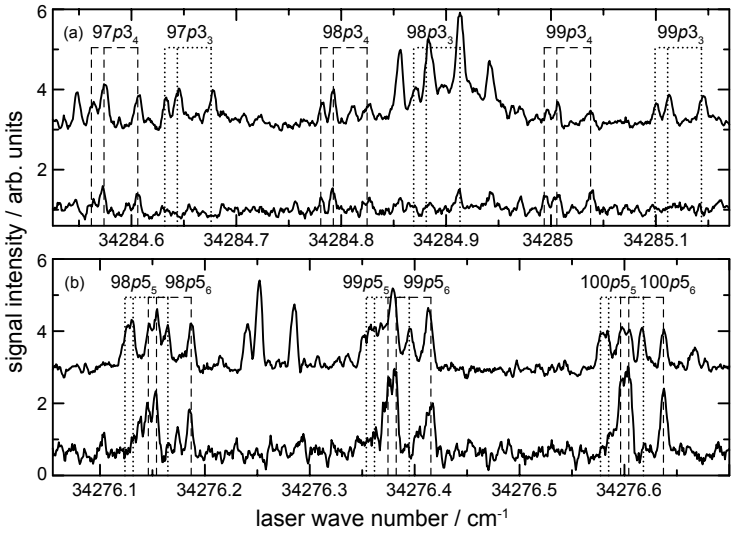

FIG. 11. Comparison between the PI spectra (top trace, shifted along the vertical axis for clarity) and the RSR-TI spectra (bottom trace) recorded (a) near the $3 \rightarrow 97$–$99p3_N$ transitions (region Q3) and (b) near the $5 \rightarrow 98$–$100p5_N$ transitions (region Q5). The calculated positions of the $N = N^+$ and $N = N^+ + 1$ Rydberg states are indicated as vertical dotted and dashed lines, respectively.

originate from the p-f interaction but may also be explained by the influence of the stray electric fields of 13 mV/cm present in the photoexcitation region. The effect of the stray field on the $N = N^+$ Rydberg states is to facilitate autoionization by inducing a $\Delta\ell = 1,\ \Delta N = 0$ interaction between the $np3_3$ ($np5_5$) Rydberg states and the $d1_3$ ($d3_5$) ionization continuum, as discussed in the context of Fig. 10 for the $41p5_5$ Rydberg state. The electric field necessary to induce such an interaction is smaller for Rydberg states around $n = 100$, because the polarizability of Rydberg states scales as n^7. The lifetimes of the $np3_4$ Rydberg states are expected to be less affected by the stray field than the $np3_3$ Rydberg state. Indeed, the $np3_4$ Rydberg states cannot decay via a $\Delta\ell = 1,\ \Delta N = 0$ interaction because the $N^+ = 1,\ \ell = 2$ ionization continuum does not possess any $N = 4$ character. The field-induced decay must therefore proceed via a $\Delta\ell = 1,\ \Delta N = 1$ rather than a (stronger) $\Delta\ell = 1,\ \Delta N = 0$ interaction. The surprisingly long lifetime of the $np5_6$ Rydberg states around $n = 100$ is a consequence of the fact that their effective quantum defects are almost zero (see Fig. 9c) and that, consequently, their positions coincide with the positions of the manifold of nonpenetrating ($\ell \geq 3$) Stark states, to which they are coupled by the p-f interaction. The stray field, though weak, therefore efficiently induces high-ℓ character to the $np5_6$ Rydberg states around $n = 100$, which prolongs their lifetimes beyond 2 μs.

TABLE VIII. Rotational energies of $^4He_2^+$ in the $X^+\,^2\Sigma_u^+$ ($v^+ = 0$) ground state relative to the $N^+ = 1$ level as determined in various studies. All values are given in units of cm^{-1}.

N^+	Ref. 18 (ZEKE)	Ref. 18 (MQDT fit)	Ref. 7 (*ab initio*)	Present work (MQDT fit)
1	0	0	0	0[a]
3	70.943(6)	70.918(3)	70.936	70.937(3)
5	198.379(16)	198.317(8)	198.359	198.369(6)
7	381.858(31)	381.761(16)	381.822	381.822[b]

[a] The term value of the $(v^+ = 0, N^+ = 1)$ ionization threshold relative to the hypothetical $(v'' = 0, N'' = 0)$ level of the $2s\sigma\, a\,^3\Sigma_u^+$ state of $^4He_2$ was determined to be $34\,316.387(10)\,cm^{-1}$, which represents the average of the results of fit A ($34\,316.391\,cm^{-1}$) and fit C ($34\,316.383\,cm^{-1}$).

[b] Fixed to the *ab initio* value of Ref. 7.

IV. CONCLUSIONS

The term values of triplet np Rydberg states with $n > 20$ converging to the $(v^+ = 0, N^+ = 1, 3, 5, 7)$ levels of the $X^+\,^2\Sigma_u^+$ ground state of $^4He_2^+$ have been obtained by Rydberg-state-resolved threshold-ionization (RSR-TI) spectroscopy. By combining the data with spectroscopic data on low-lying triplet np and nf Rydberg states from the literature[22–29] a new set of energy- and R-dependent eigenquantum-defect parameters of multichannel quantum-defect theory was derived using a methodology established by Ch. Jungen and his coworkers[40,45–54]. The MQDT model includes the effects of p-f and rovibrational channel interactions and provides an accurate description of all triplet np and nf Rydberg states of He_2 with $v^+ \leq 2$ and $N^+ \leq 9$ ($N^+ \leq 19$ for states with negative electronic parity). The root-mean-square deviation between observed and calculated term values was $0.005\,cm^{-1}$ for the Rydberg states measured in this investigation ($n > 20$) and $0.2\,cm^{-1}$ for the low-n Rydberg states taken from the literature ($n = 2$–20). These deviations correspond to the experimental uncertainties of the respective measurements.

The adjusted eigenquantum-defect functions were combined with the potential energy function of the ground electronic state of He_2^+ from Ref.[7] to derive the Born-Oppenheimer potential-energy functions and the leading adiabatic corrections of the triplet np Rydberg states of He_2 with $n \leq 5$ in the range of internuclear distances $R = 1.7$–$2.7\,a_0$. It will be interesting in future to compare these results with potential-energy curves obtained by *ab initio* quantum chemistry.

Rotational spectroscopy on $^4He_2^+$ at an accuracy of up to $0.003\,cm^{-1}$ was performed

by extrapolating the experimental term values of triplet np Rydberg states in the range $n = 87$–110 to their ionization limit using MQDT. The resulting positions of the lowest rotational levels of $^4He_2^+$ are compared to previous results from the literature in Table VIII. The energy of the $(v^+ = 0, N^+ = 3)$ rotational level is in excellent agreement with the latest *ab initio* calculations[7] and the value obtained by ZEKE spectroscopy.[18] A deviation on the order of six standard deviations is found with the latest value extrapolated from the energies of Rydberg states.[18] The reason for this deviation lies presumably in the neglect of p-f and vibrational channel interactions in the MQDT model used in Ref. 18. For the energy of the $(v^+ = 0, N^+ = 5)$ rotational level of $^4He_2^+$ we find a small deviation with the *ab initio* calculations from Ref. 7. The deviation might result from systematic dc Stark shifts of the high-n Rydberg states around $n = 100$ used to extrapolate the rotational energies in the present study. Alternatively, it may reflect the neglect of quantum-electrodynamics corrections in the *ab initio* calculations of the rotational energies. Such corrections were found to be significant in H_2.[61,62] Our result is in good agreement with, but more accurate than, the result obtained by ZEKE spectroscopy[18] but deviates significantly from the latest value extrapolated from the energies of Rydberg states,[18] a deviation we also attribute to the incomplete nature of the MQDT model used in Ref. 18.

The delayed pulsed-field ionization of Rydberg states in RSR-TI spectroscopy restricts the detection to long-lived Rydberg states only. The autoionization dynamics of the triplet $np\,(v^+ = 0)$ Rydberg states with $N = N^+$ and $N = N^+ + 1$ was found to be governed by the p-f interaction, which reduces the lifetimes to values below $2\,\mu$s for levels with $n \lesssim 90$. The $41p5_5$ Rydberg states has an exceptionally long lifetime of $> 2\,\mu$s because of the p-f interaction with the long-lived $23f7_5$ Rydberg state. At higher n values, the stray electric field of $\sim 13\,$mV/cm induces N- and ℓ-mixing and governs the autoionization dynamics. The field-induced interactions can lead to shorter or longer lifetimes, depending on whether the interaction is with an ionization continuum or with long-lived Rydberg states.

ACKNOWLEDGMENTS

We dedicate this article to Christian Jungen (Laboratoire Aimé Cotton du CNRS, Orsay) and thank him for useful discussions and for allowing us to use his MQDT program. DS and FM also thank him and the Laboratoire Aimé Cotton for numerous research periods in

Orsay. We thank Matthias Raunhardt for his help in the operation of the discharge used to generate metastable He_2. This work was supported financially by the Swiss National Science Foundation under project 200020-146759 and by the European Research Council advanced grant program under project 228286.

REFERENCES

[1]T. M. Miller, in *CRC Handbook of Chemistry and Physics, 94th Edition*, edited by W. M. Haynes (CRC Press/Taylor and Francis, Boca Raton, FL, Internet Version 2014).

[2]D. Z. Kandula, Ch. Gohle, T. J. Pinkert, W. Ubachs, and K. S. E. Eikema, Phys. Rev. Lett. **105**, 063001 (2010).

[3]F. Grandinetti, Int. J. Mass Spectrom. **237**, 243 (2004).

[4]F. Luo, G. C. McBane, G. Kim, C. F. Giese, and W. R. Gentry, J. Chem. Phys. **98**, 3564 (1993).

[5]W. Schöllkopf and J. P. Toennies, Science **266**, 1345 (1994).

[6]W. Cencek, , M. Przybytek, J. Komasa, J. B. Mehl, B. Jeziorski, and K. Szalewicz, J. Chem. Phys. **136**, 224303 (2012).

[7]W.-C. Tung, M. Pavanello, and L. Adamowicz, J. Chem. Phys. **136**, 104309 (2012).

[8]C. W. Bauschlicher, Jr., H. Partridge, and D. Ceperley, Chem. Phys. Lett. **160**, 183 (1989).

[9]J. Ackermann and H. Hogreve, Chem. Phys. **157**, 75 (1991).

[10]W. Cencek and J. Rychlewski, J. Chem. Phys. **102**, 2533 (1995).

[11]A. Carrington, C. H. Pyne, and P. J. Knowles, J. Chem. Phys. **102**, 5979 (1995).

[12]F. X. Gadéa and I. Paidarová, Chem. Phys. **209**, 281 (1996).

[13]W. Cencek and J. Rychlewski, Chem. Phys. Lett. **320**, 549 (2000).

[14]J. Xie, B. Poirier, and G. I. Gellene, J. Chem. Phys. **122**, 184310 (2005).

[15]M. Stanke, D. Kędziera, S. Bubin, M. Molski, and L. Adamowicz, Phys. Rev. A **76**, 052506 (2007).

[16]A. Ruzsinszky, J. P. Perdew, G. I. Csonka, O. A. Vydrov, and G. E. Scuseria, J. Chem. Phys. **126**, 104102 (2007).

[17]N. Yu and W. H. Wing, Phys. Rev. Lett. **59**, 2055 (1987).

[18]M. Raunhardt, M. Schäfer, N. Vanhaecke, and F. Merkt, J. Chem. Phys. **128**, 164310

(2008).

[19]L. Coman, M. Guna, L. Simons, and K. A. Hardy, Phys. Rev. Lett. **83**, 2715 (1999).

[20]W. J. van der Zande and W. Ubachs, Phys. Rev. Lett. **84**, 3212 (2000).

[21]K. Hardy and X. W. Wang, Phys. Rev. Lett. **84**, 3213 (2000).

[22]D. S. Ginter, M. L. Ginter, and C. M. Brown, J. Chem. Phys. **81**, 6013 (1984).

[23]D. S. Ginter and M. L. Ginter, J. Mol. Spectrosc. **82**, 152 (1980).

[24]F. B. Orth and M. L. Ginter, J. Mol. Spectrosc. **64**, 223 (1977).

[25]F. B. Orth and M. L. Ginter, J. Mol. Spectrosc. **61**, 282 (1976).

[26]C. M. Brown and M. L. Ginter, J. Mol. Spectrosc. **40**, 302 (1971).

[27]G. Herzberg and Ch. Jungen, J. Chem. Phys. **84**, 1181 (1986).

[28]C. Focsa, P. F. Bernath, and R. Colin, J. Mol. Spectrosc. **191**, 209 (1998).

[29]K. Kawaguchi, Y. Hama, and S. Nishida, J. Mol. Spectrosc. **232**, 1 (2005).

[30]D. N. McKinsey, C. R. Brome, J. S. Butterworth, S. N. Dzhosyuk, P. R. Huffman, C. E. H. Mattoni, J. M. Doyle, R. Golub, and K. Habicht, Phys. Rev. A **59**, 200 (1999).

[31]R. Seiler, Th. Paul, M. Andrist, and F. Merkt, Rev. Sci. Instr. **76**, 103103 (2005).

[32]R. Seiler, U. Hollenstein, G. M. Greetham, and F. Merkt, Chem. Phys. Lett. **346**, 201 (2001).

[33]R. Seiler, U. Hollenstein, T. P. Softley, and F. Merkt, J. Chem. Phys. **118**, 10024 (2003).

[34]U. Hollenstein, R. Seiler, and F. Merkt, J. Phys. B: At. Mol. Opt. Phys. **36**, 893 (2003).

[35]S. Gerstenkorn, J. Vergès, and J. Chevillard, *Atlas du Spectre d'Absorption de la Molécule d'Iode: 11 000–14 000 cm*$^{-1}$ (Laboratoire Aimé-Cotton CNRS II, Orsay, 1982).

[36]D. Sprecher, J. Liu, Ch. Jungen, W. Ubachs, and F. Merkt, J. Chem. Phys. **133**, 111102 (2010).

[37]J. Liu, E. J. Salumbides, U. Hollenstein, J. C. J. Koelemeij, K. S. E. Eikema, W. Ubachs, and F. Merkt, J. Chem. Phys. **130**, 174306 (2009).

[38]C. R. Mahon, G. R. Janik, and T. F. Gallagher, Phys. Rev. A **41**, 3746 (1990).

[39]F. Merkt, H. H. Fielding, and T. P. Softley, Chem. Phys. Lett. **202**, 153 (1993).

[40]G. Herzberg and Ch. Jungen, J. Mol. Spectrosc. **41**, 425 (1972).

[41]F. Merkt and T. P. Softley, Phys. Rev. A **46**, 302 (1992).

[42]J. W. C. Johns and D. W. Lepard, J. Mol. Spectrosc. **55**, 374 (1975).

[43]W. A. Chupka, J. Chem. Phys. **98**, 4520 (1993).

[44]F. Merkt and R. N. Zare, J. Chem. Phys. **101**, 3495 (1994).

[45]Ch. Jungen and O. Atabek, J. Chem. Phys. **66**, 5584 (1977).

[46]C. H. Greene and Ch. Jungen, Adv. At. Mol. Phys. **21**, 51 (1985).

[47]S. C. Ross and Ch. Jungen, Phys. Rev. A **49**, 4353 (1994).

[48]S. C. Ross and Ch. Jungen, Phys. Rev. A **49**, 4364 (1994).

[49]S. C. Ross and Ch. Jungen, Phys. Rev. A **50**, 4618 (1994).

[50]S. C. Ross, Ch. Jungen, and A. Matzkin, Can. J. Phys. **79**, 561 (2001).

[51]Ch. Jungen, K. P. Huber, M. Jungen, and G. Stark, J. Chem. Phys. **118**, 4517 (2003).

[52]A. Osterwalder, A. Wüest, F. Merkt, and Ch. Jungen, J. Chem. Phys. **121**, 11810 (2004).

[53]M. Glass-Maujean and Ch. Jungen, J. Phys. Chem. A **113**, 13124 (2009).

[54]Ch. Jungen, *Elements of quantum defect theory* in *Handbook of High-resolution Spectroscopy*, edited by M. Quack and F. Merkt (John Wiley & Sons, Ltd., 2011).

[55]D. Sprecher, Ch. Jungen, and F. Merkt, J. Phys. Chem. A **117**, 9353 (2013).

[56]L. Wolniewicz, J. Mol. Spectrosc. **174**, 132 (1995).

[57]W. Kołos and J. Rychlewski, J. Mol. Spectrosc. **177**, 146 (1996).

[58]G. Staszewska and L. Wolniewicz, J. Mol. Spectrosc. **198**, 416 (1999).

[59]G. Staszewska, J. Phys. Chem. A **105**, 2308 (2001).

[60] See supplementary material at http:// for tables containing experimental term values of triplet np Rydberg states of He_2 taken from the literature and their comparison to MQDT calculations.

[61]J. Komasa, K. Piszczatowski, G. Łach, M. Przybytek, B. Jeziorski, and K. Pachucki, J. Chem. Theory Comput. **7**, 3105 (2011).

[62]E. J. Salumbides, G. D. Dickenson, T. I. Ivanov, and W. Ubachs, Phys. Rev. Lett. **107**, 043005 (2011).